4-2016

Modifications to Johanson's roll compaction model for improved relative density predictions

Yu Liu
Purdue University

Graduate School Form
30 Updated 12/26/2015

PURDUE UNIVERSITY
GRADUATE SCHOOL
Thesis/Dissertation Acceptance

This is to certify that the thesis/dissertation prepared

By Yu Liu

Entitled

MODIFICATIONS TO JOHANSON'S ROLL COMPACTION MODEL FOR IMPROVED RELATIVE DENSITY PREDICTIONS

For the degree of Master of Science in Mechanical Engineering

Is approved by the final examining committee:

Carl Wassgren
Chair

Michael Harris
Co-chair

Marcial Gonzalez
Co-chair

To the best of my knowledge and as understood by the student in the Thesis/Dissertation Agreement, Publication Delay, and Certification Disclaimer (Graduate School Form 32), this thesis/dissertation adheres to the provisions of Purdue University's "Policy of Integrity in Research" and the use of copyright material.

Approved by Major Professor(s): Carl Wassgren

Approved by: Jay Gore 4/18/2016

Head of the Departmental Graduate Program Date

MODIFICATIONS TO JOHANSON'S ROLL COMPACTION MODEL FOR IMPROVED RELATIVE DENSITY PREDICTIONS

A Thesis

Submitted to the Faculty

of

Purdue University

by

Yu Liu

In Partial Fulfillment of the

Requirements for the Degree

of

Master of Science in Mechanical Engineering

May 2016

Purdue University

West Lafayette, Indiana

For my family

ACKNOWLEDGEMENTS

I would like to thank those who helped me though the process of completing this thesis. First, I would like to express the deepest appreciation to Prof. Carl Wassgren, my major professor, who guided me and supported me to grow as a researcher. Without his guidance and persistent help this thesis would not have been possible. Thanks to Prof. Marcial Gonzalez and Prof. Michael T. Harris for their service as my committee members. Thanks to the whole research group who gave me suggestions and ideas. Specially, I greatly appreciate the Abaqus guidance and density-dependent DPC data (Tables 3.4 and 3.5) collected by Shrikant Swaminathan at Purdue University.

I am also grateful to the National Science Foundation Engineering Research Center for Structured Organic Particulate Systems (NSF ERC-SOPS, 0951845-EEC) for financial support.

In addition, I want to thank my family, my girlfriend and all friends for their support and love, without them I would not be able to do anything.

TABLE OF CONTENTS

Page

LIST OF TABLES

Table Page

LIST OF FIGURES

Figure Page

Appendix Figure

NOMENCLATURE

α	nip angle
θ	position angle
η	relative density
η_{initial}	relative density at the inlet
η_{θ}	relative density at the position angle θ
η_{α}	relative density at the nip angle α
η_0	relative density at the position angle 0 (minimum gap)
ε_{vol}^{pl}	total volumetric plastic strain
V	volume
S	minimum gap width between the rolls
D	roll diameter
W	roll width
ΔL	small displacement
P	pressure
P_{initial}	pressure at the inlet
P_{θ}	pressure density at the position angle θ
P_{α}	pressure density at the nip angle α
P_0	pressure density at the position angle 0 (minimum gap)

K	compressibility constant
F	roll force
σ_θ	maximum principal stress at the position angle θ
δ	effective angle of internal friction
f	mass correction factor
f_θ	mass correction factor at the position angle θ
f_0	mass correction factor at the position angle 0 (minimum gap)
β	angle of friction in the DPC model
ϕ	angle of internal friction in the Mohr-Coulomb model
d	cohesion in the DPC model
c	cohesion in the Mohr-Coulomb model

ABSTRACT

Liu, Yu. M.S.M.E., Purdue University, May 2016. Modifications to Johanson's Roll Compaction Model for Improved Relative Density Predictions. Major Professor: Carl Wassgren, School of Mechanical Engineering.

Johanson's roll compaction model [J.R. Johanson, A rolling theory for granular solids, ASME Journal of Applied Mechanics E32 (1965) 842–848] is modified to improve its predictions of a compacted ribbon's relative density. Previous work has shown that the maximum roll pressure and ribbon relative density predicted by the Johanson model are not only larger than those predicted from finite element method (FEM) simulations, but also unphysical in some cases. This over-prediction is due to a one-dimensional flow assumption in the Johanson model. Real velocity profiles have been shown to be non-uniform.

Johanson's analysis is modified in this work to include a mass correction factor to account for the improper one-dimensional flow assumption, similar to what was proposed by Bi et al. [M. Bi, F. Alvarez-Nunez, F. Alvarez, Evaluating and modifying Johanson's rolling model to improve its predictability, J Pharm Sci. 103 (2014), 2062-2071]. Unlike Bi et al.'s work, however, an empirical curve fit for the mass correction factor is included in the current analysis. Two fitting parameters, found from an on-line measurement of the roll force and minimum roll gap, are used to determine the mass correction factor at the minimum gap width.

Predictions of the average relative density at the minimum gap width from the modified Johanson model are compared to predictions from two-dimensional FEM models and the errors are found to be around 5% of the FEM predictions. The unmodified Johanson model over-predicts the FEM results by around 50%. Comparisons to published experimental data also show good agreement. This modified Johanson model can be used in control schemes to provide much better estimates of ribbon relative density in roll compaction operations.

CHAPTER 1. INTRODUCTION

Roll compaction is a widely used unit operation during the production of powder-based products in the pharmaceutical, chemical, consumer products, ceramics, and food industries. Roll compaction is a dry granulation process in which loose powder is compressed to produce a continuous, compacted ribbon with non-zero porosity. The resulting ribbon is typically processed further, for example by milling into granules, blending with other materials, and compacting into tablets (Figure 1.1).

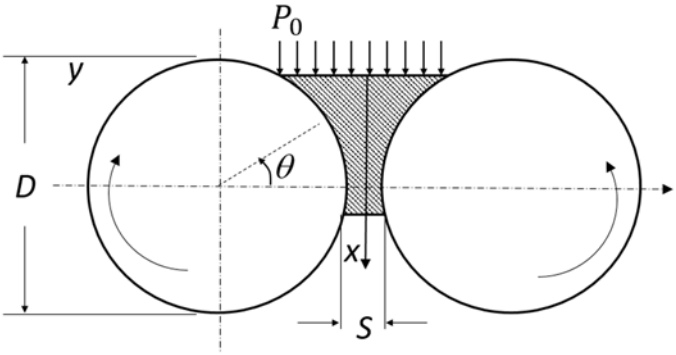

Figure 1.1. Roll compacting.

A roll compaction parameter of particular interest is the resulting ribbon's bulk density distribution. Most other ribbon properties, such as elastic modulus, Poisson's ratio, and fracture strength, are functions of the bulk density. In addition, since the ribbon is usually milled into granules, the granule distribution properties are strong functions of the ribbon properties. These granule properties are known to have significant influence

on the resulting product properties, such as disintegration and compact strength [1]. Thus, having the ability to predict and control the ribbon bulk density distribution is of significant interest.

Although roll compaction has been used extensively within industry, the process is still often designed using empirical methods. Design of experiments (DOE) approaches are not uncommon despite a number of mechanistic models for the process being available since the 1960s. The one-dimensional model of Johanson [2] is perhaps the most commonly cited roll compaction model, but the “slab” method [3] has also been proposed. Computational finite element method (FEM) models for roll compaction [4-8] are becoming more common and can provide extensive information on the powder state, but at the expense of increased complexity and calculation time. The reliance on empirical studies may be due in part to the inaccuracy of one-dimensional model predictions, which is discussed in greater detail in the following section, and the effort and experience needed to implement an FEM model.

The current work focuses on improving the prediction of the average ribbon relative density from the Johanson model [2]. An approach to correct for the one-dimensional flow assumption made by Johanson is included in the ribbon relative density analysis. Predictions from this modified model are compared to two-dimensional and three-dimensional FEM simulation results and published experimental data.

CHAPTER 2. BACKGROUND

Although other roll compaction mechanistic modeling approaches have been proposed, the Johanson model [2] is the most commonly used one and, hence, is the focus of the current study. The model is one-dimensional and does not require significant computational resources; hence, it is ideal for initial design calculations and control schemes. At the other end of the computational spectrum are finite element method (FEM) models, which can be multi-dimensional and provide detailed powder state information, but at the expense of increased model development and computational effort. The remainder of this chapter gives a general description of the Johanson model along with comparisons to FEM simulations and experimental measurements.

Details of the Johanson model derivation are provided in Chapter 5, but it is worthwhile to state here the major assumptions of the model and its capabilities. The roll geometry is assumed known, which is reasonable. The stress at the inlet to the slip region is also assumed known, but this is generally not true in practice. Little effort has been invested into predicting this inlet stress, although there has been recent work [9] relating the torque of a feed screw leading into the rolls to the inlet stress. The powder in the model was assumed by Johanson to be isotropic, frictional, cohesive, compressible, and obey the Jenike-Shield yield criterion [10]. Johanson further proposed that the powder's relative density is related to the applied stress via a power law relationship, which fits

many experimental measurements [11]. Additional powder properties used in the model include the effective angle of internal friction and the powder-roll friction angle, both of which are assumed constant with relative density, which is reasonable at the large stresses expected in a roll compactor [5].

Johanson assumed that powder flow through the roll compactor is one-dimensional, with a speed less than the roll speed in the upstream “slip” region and equal to the roll speed in the downstream “no-slip” region. The transition between regions occurs at the “nip” angle, which is calculated in the Johanson model by equating powder stress gradients in the two different regions. Once in the no-slip region, the powder relative density is found through simple geometry and the corresponding applied stress is determined using the aforementioned power law constitutive relationship. In addition to the nip angle, the Johanson model can be used to predict the final ribbon relative density at the minimum gap and the force and torque acting on the rolls.

Several experimental studies have attempted to validate the Johanson model. For example, Bindhumadhavan et al. [12] found that the predicted nip angle agreed with experimental measurements to within 15%. Yusof et al. [13] also noted reasonable agreement between experiments and model predictions of the roll force, but only for roll gaps smaller than 0.15 mm. The latter authors also noted that a slight change in the initial bulk porosity had a large effect on the calculated roll force, which did not agree with experiment results.

Recent two-dimensional FEM simulation studies by Muliadi et al. [5] found that the Johanson model produces reasonable nip angle predictions. However, the Johanson model over-predicts the maximum roll pressure and ribbon relative density significantly,

and in many cases predicts relative densities greater than one, which is non-physical. The cause for the poor relative density predictions was because powder flow through the roll compactor is not one-dimensional. Indeed, the powder speed in the no-slip region is fastest at the rolls and slowest at the centerline. Similar observations were made in the FEM studies by Cunningham [7] and Zavaliangos et al. [14], and in the experiments by Orowan [15]. As noted by Muliadi et al. [5], because Johanson assumes one-dimensional flow with a speed equal to the roll speed, the mass flow rate through the system is larger than what actually occurs. As a result, the ribbon relative density is over-predicted.

The objective of the current work is to improve the ribbon relative density predictions of the Johanson model by modifying its analysis to correct for the assumption of one-dimensional flow. The approach used here is similar to the one proposed recently by Bi et al. [16], who make use of a mass correction factor. The implementation here, however, is different and is described in detail in Chapter 5. Chapter 5 also compares the modified Johanson model predictions to two-dimensional FEM simulation results and published experimental data. Details of these FEM models are given in the following chapter.

CHAPTER 3. TWO-DIMENSIONAL FINITE ELEMENT MODEL

3.1 Introduction

A two-dimensional FEM model is used here to provide: (a) insights into the form of the mass correction factor relation described in Chapter 5, and (b) a means of validation, albeit a computational one rather than an experimental one. Prior studies [6-8] have shown that FEM models can provide good predictions of the ribbon relative density. The commercial FEM package Abaqus/Explicit V6.14 is used in the current study to perform the simulations.

3.2 Model Description

3.2.1 Model Assumptions and Boundary Conditions

The FEM model used here is derived from the one described by Muliadi et al. [5]. The system geometry is shown in Figure 3.1 and mimics an Alexanderwerks Model WP 200 PHARMA lab-scale roll compactor with 200 mm diameter rollers and a minimum gap width of up to 5 mm.

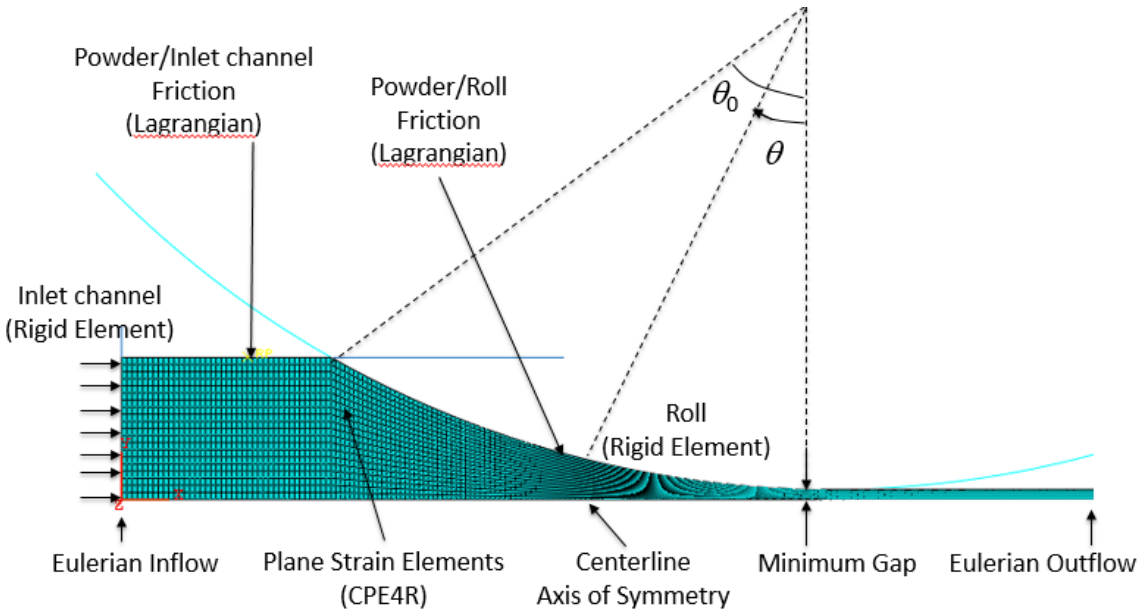

Figure 3.1. A schematic of the geometry modeled in the two-dimensional FEM simulations.

As shown in Figure 3.1, several assumptions are made in the current two-dimensional FEM model: (1) the simulation process is quasi-static, (2) interstitial air and gravity are not included in the model, (3) the roll and inlet channel boundaries are assumed to be non-deformable, frictional, Lagrangian boundaries, (4) the lower boundary is a plane of symmetry to save computation time, (5) within the domain, powder is modeled using CPE4R elements (reduced integration, plane strain elements), and (6) Eulerian boundary conditions are used at the inlet and outlet so that material can flow continuously through the domain.

Considering the significant size change between the inlet and minimum roll gap, a mixed Lagrangian-Eulerian mapping method, also known as the arbitrary Lagrangain-Eulerian (ALE) scheme, is applied to the computational domain. By using this coordinate mapping method, both the Eulerian and Lagrangain boundaries can be applied to the

computational domain and significant distortion can be handled by re-meshing the entire domain continuously during the simulation.

A specified uniform normal stress is applied at the inlet boundary, consistent with what is used in the Johanson model. Coulomb sliding friction, with a constant friction coefficient, is applied at the roll and inlet channel surfaces, again, consistent with the Johanson model. The roller rotates at a constant speed of 1 rad/s (9.55 rpm). Unlike the FEM model of Cunningham [7] and Muliadi et al. [5], the computational domain in the current study has a longer release region, i.e., the region downstream of the minimum gap. Muliadi et al. [5] showed that the maximum roll normal stress in FEM simulations occurs at a location slightly upstream of the minimal gap, which is different from the Johanson model's assumption that the maximum roll normal stress occurs at the minimum gap. However, not only does this location vary depending on the material properties and boundary conditions, as found by Muliadi et al., but it has also been found in the current work to depend on the length of the release region. As shown in Table 3.1, as the release region length increases, the location of the maximum roll normal stress moves further downstream until it eventually occurs at the minimum gap location, consistent with Johanson's assumption. Therefore, in order to better simulate the roll compaction process, a longer released region is chosen in this study such that it does not affect the simulation results.

Table 3.1. The angle of the maximum roll normal stress as measured from the minimum gap location as a function of the length of the release region (refer to Figure 3.1). The inlet stress, gap width, roll diameter, and powder-roll friction angle for the simulations are, respectively, 100 kPa, 3 mm, 200 mm and 0.5. The remainder of the material properties are given in Tables 3.2 and 3.3.

Length of the release region, l_3 (mm)	0	5	10	15	20
Angle of the maximum roll normal stress, θ (degree)	1.72	0.86	0.29	0	0

3.2.2 Material Properties

To describe the powder continuum stress-strain behavior, the powder is modeled using the Drucker-Prager/Cap (DPC) plasticity model. Details of the DPC model, including experimental calibration of the model parameters, can be found in works by Michrafy et al. [17] and Sinha et al. [18]. Note that this constitutive model assumes quasi-static behavior and does not include the effects of interstitial air. In the current study, density-independent DPC parameters are used in most of the simulations to compare with theoretical results since the Johanson model also assumes constant properties. Comparisons to density-dependent properties used within both two- and three-dimensional FEM simulations, are discussed in Chapter 5. The specific density-independent DPC powder properties used in these studies are provided in Tables 3.2 and 3.3 and correspond to a particular brand of microcrystalline cellulose (Avicel PH-102, FMC-BioPolymer, PA, USA) as reported by Muliadi et al. [5]. The density-dependent DPC properties used in simulations for the same material were collected by Swaminathan et al. [19] and are given in Tables 3.4 and 3.5.

Table 3.2. Density-independent cap plasticity and elastic parameters for the simulated powder.

Cohesion (MPa)	Friction angle (degree)	Cap eccentricity	Young's modulus (MPa)	Poisson's ratio
0.127	56.5	0.166	481	0.062

Table 3.3. Density-independent cap hardening parameters for the simulated powder.

Volumetric plastic strain	0	0.257	0.478	0.662	0.814	0.950	1.070	1.140
Hydrostatic yield stress (MPa)	0.04	1.61	4.08	12.00	23.07	42.30	79.60	143.0

Table 3.4. Density-dependent cap plasticity and elastic parameters for the simulated powder.

Relative density	Cohesion (MPa)	Friction angle (degree)	Cap eccentricity	Young's modulus (MPa)	Poisson's ratio
0.411	0.293	68.87	0.320	519	0.100
0.492	1.15	67.37	0.331	689	0.106
0.589	4.28	67.95	0.357	982	0.115
0.686	6.15	64.93	0.381	1140	0.129
0.783	11.8	62.61	0.465	2770	0.144
0.881	15.8	65.82	0.599	5610	0.170

Table 3.5. Density-dependent cap hardening parameters for the simulated powder.

Volumetric plastic strain	0.280	0.458	0.639	0.791	0.923	1.041
Hydrostatic yield stress (MPa)	5.31	7.72	13.70	23.70	41.40	78.00

In order to compare to the maximum relative density predictions of the Johanson model, the material relative density at the minimum gap location is calculated in the FEM model using the total volumetric plastic strain as proposed by Gurson [20],

$$\rho_{\theta=0} = \rho_{\text{initial}} \exp\left(-\varepsilon_{vol}^{pl}\Big|_{\theta=0}\right), \tag{3.1}$$

where η_{initial} is the relative density at the inlet (= 0.311), which is the initial relative density downstream of the feeder [6-8]. As is shown in Chapter 5, the inlet pressure used in the current work is smaller than the pressure corresponding to the tapped relative density. Thus, the powder at the inlet is in an uncompressed state. The quantity $\varepsilon_{\text{vol}}^{\text{pl}}$ is the total volumetric plastic strain (PEQC4 value in Abaqus).

3.3 Results and Discussion

The grid independence verification of two-dimensional FEM models has been done by Muliadi et al. [5]. Since the same model is used in the current study, there is no need to repeat this verification. For convenience, the result is listed here in Table 3.6. As shown in Table 3.6, the FEM model element resolution is sufficiently fine to have negligible effect on the model results.

Table 3.6. Grid independence test result from Muliadi et al. [5].

Number of Elements	Maximum roll pressure P_0 (MPa)	Maximum ribbon relative density η_0
5000	63.0	0.765
7500	62.5	0.764
10,000	62.4	0.762

Also, it is found in the current study that the mass scaling, which is used by Abaqus/Explicit to improve computational efficiency, was shown to have little influence on the current FEM results, especially the velocity fields. Generally, a larger mass scaling factor can result in a more stable velocity profile. According to the Abaqus User's Manual [21], inertia force is introduced when adding mass scaling; hence, the kinetic energy should be monitored to ensure that the ratio of kinetic energy to internal energy does not exceed a certain value—typically less than 1%. The result is summarized in Table 3.7. The results show that for a mass scaling factor less than 500, the ratio of kinetic energy to internal energy is less than 0.1%. Hence, a proper mass scaling factor is chosen to get a stable velocity profile while increasing computational efficiency without degrading accuracy.

Table 3.7. Mass scaling study results. The inlet stress, minimum gap width, roll diameter, and powder-roll friction coefficient are, respectively, 100 kPa, 4 mm, 200 mm, and 0.55. The remainder of the material properties are given in Tables 3.2 and 3.3.

Mass scaling factor	Kinetic energy KE (J)	Internal energy IE (J)	KE/IE
0	0.0564	30335	1.86E-06
50	2.8645	28690	9.98E-05
500	28.4579	27590	1.03E-03

An example two-dimensional FEM simulation is performed to provide insights into the roll compaction process. The inlet stress, minimum gap width, roll diameter, and powder-roll friction coefficient for this special case are, respectively, 200 kPa, 4 mm, 200 mm, and 0.3. The resulting friction coefficients across the powder-roll face are shown in Figure 3.2 by monitoring roll normal and shear stresses. The shape of the powder-roll

friction coefficient curve is similar to those obtained by Cunningham [7] and Muliadi et al. [5].

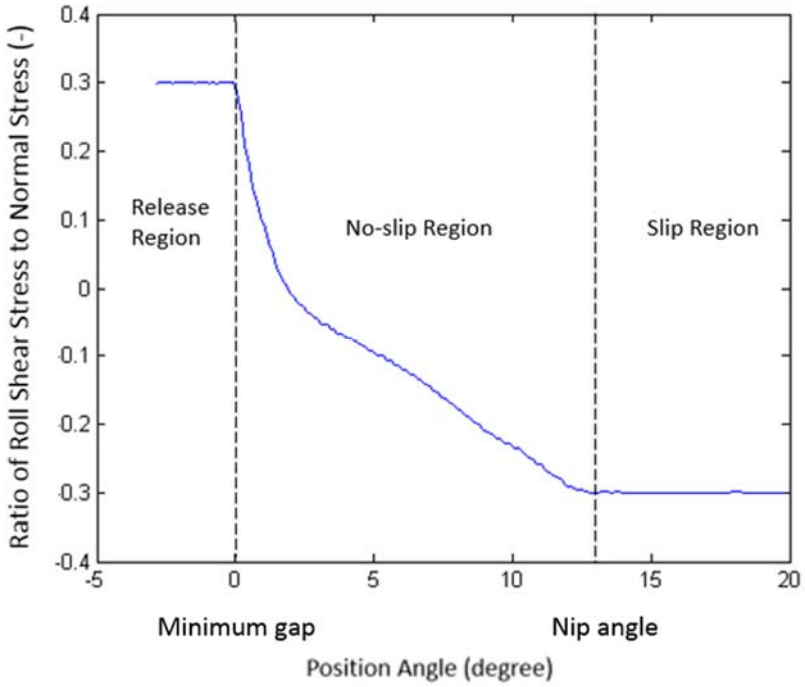

Figure 3.2. The ratio of roll shear stress to roll normal stress as a function of position angle for the example simulation. The inlet stress, minimum gap width, roll diameter, and powder-roll friction coefficient are, respectively, 200 kPa, 4 mm, 200 mm, and 0.3. The remainder of the material properties are given in Tables 3.2 and 3.3.

Through Figure 3.2, identification of the slip region, no-slip region, and release regions can be easily performed by studying the friction coefficient, i.e., the ratio of roll shear stress to roll normal stress. Recall that Coulomb sliding friction, with a constant friction coefficient, is applied at the powder-roll surface, so slipping occurs when

$$\tau_{\text{roll}} = \mu_{\text{roll}} \sigma_{\text{roll}} . \tag{3.2}$$

Figure 3.2 shows clearly: (1) a slip region close to the entry where the powder slips along the roll surface, (2) a no-slip region where the powder sticks to the roll surface,

and (3) a release region where spring-back occurs and the powder moves faster than the roll.

Figure 3.3 shows the velocity profile predicted by the FEM model for the example simulation. The result indicates that the material close to roll surface moves faster than the material at the centerline and the velocity becomes more uniform downstream. Hence, the one-dimensional flow assumption in Johanson's model is improper and needs to be modified.

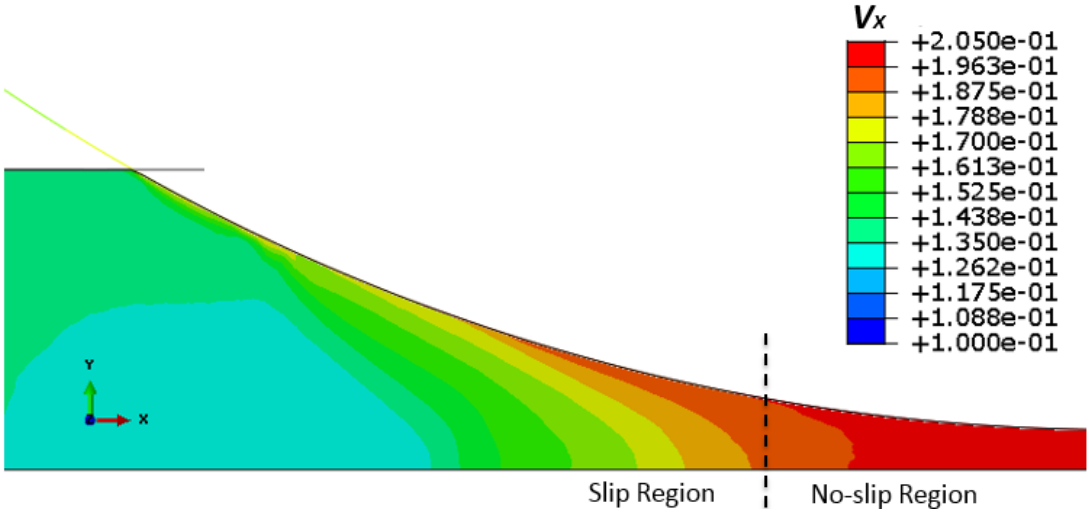

Figure 3.3. Streamwise component of the powder velocity generated from the example FEM simulation. The inlet stress, minimum gap width, roll diameter, and powder-roll friction coefficient are, respectively, 200 kPa, 4 mm, 200 mm, and 0.3. The remainder of the material properties are given in Tables 3.2 and 3.3.

3.4 Conclusions

A two-dimensional FEM model of the powder roll compaction is developed. Details of the model assumptions, boundary conditions, and material properties are given in this chapter. The simulation results show that the one-dimensional flow assumption in the Johanson model is improper and need to be modified.

CHAPTER 4. THREE-DIMENSIONAL FINITE ELEMENT MODEL

4.1 Introduction

Previous works [6-8] have shown that in reality there is a variation in stress and density distributions along the ribbon spanwise direction, which is ignored in one-dimensional and two-dimensional models. Moreover, powder-cheekplate friction may play an important role in downstream ribbon density distributions. To explore the effect of this variation in the current work, a three-dimensional FEM model is developed and the simulation results are discussed in this chapter.

4.2 Model Description

The three-dimensional model is built from the two-dimensional model discussed previously and details can be found in Chapter 3. Only the differences are discussed here.

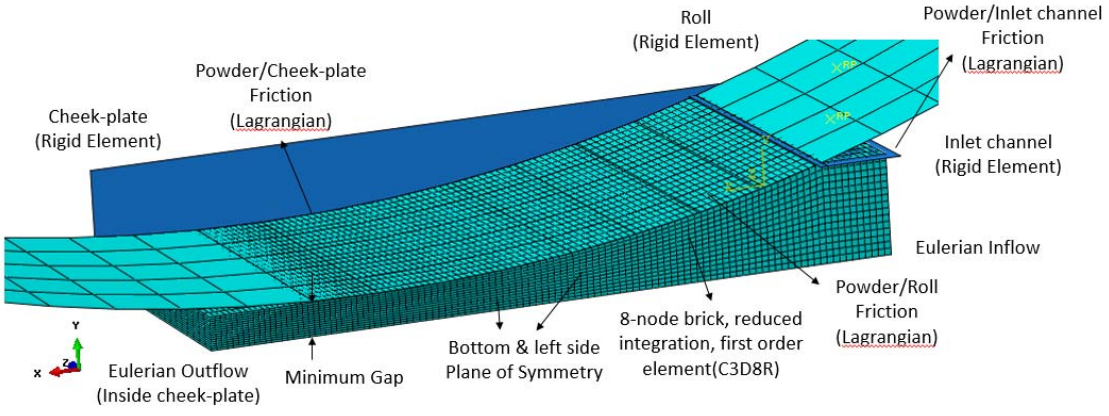

Figure 4.1. A schematic of the geometry modeled in the 3-D FEM simulations.

Figure 4.1 shows the key assumptions and boundary conditions. Note that to be computationally efficient, only one quarter of the real geometry is modeled due to the bottom and left side symmetric planes. Eulerian inflow and outflow are introduced the same way as the two-dimensional model. Within the computational domain, powder is modeled using C3D8R element (8-node brick, reduced integration, first order element). The Arbitrary Lagrangain-Eulerian (ALE) scheme is employed also to handle the non-linear contact conditions and large mesh distortion. Besides the roll and inlet channel, a cheekplate is added to the right side and Coulomb sliding friction is applied. The system geometry mimics a lab-scale roll compactor (model TF-Mini, Vector Corporation, Marion, IA) with 100 mm diameter and 20 mm width rollers.

Again, the powder mechanical behavior is described using the Drucker-Prager/Cap (DPC) plasticity model. Both the density-independent (Tables 3.2 and 3.3) and density-dependent (Tables 3.4 and 3.5) material parameters can be applied to help better investigate the powder state. Note that an external user-defined subroutine VUSDFLD [21] needs to be implemented if density-dependent parameters are used. Details on this subroutine can be found in the work done by Muliadi et al. [6].

4.3 Results and Discussion

As mentioned previously, the powder-cheekplate friction can lead to variations in stress and density distributions along the roll width direction. Hence, it is worth exploring the transverse variation to investigate the influence of powder-cheekplate friction.

As shown in Figure 4.2, both the roll normal stress and ribbon relative density increase along the downstream direction until reaching the maximum value at the minimum roll gap. As expected, the roll normal stress and ribbon relative density vary

along the ribbon spanwise direction with a non-zero powder-cheekplate friction coefficient. Note here only half of the ribbon width is shown due to the side symmetric boundary.

(a)

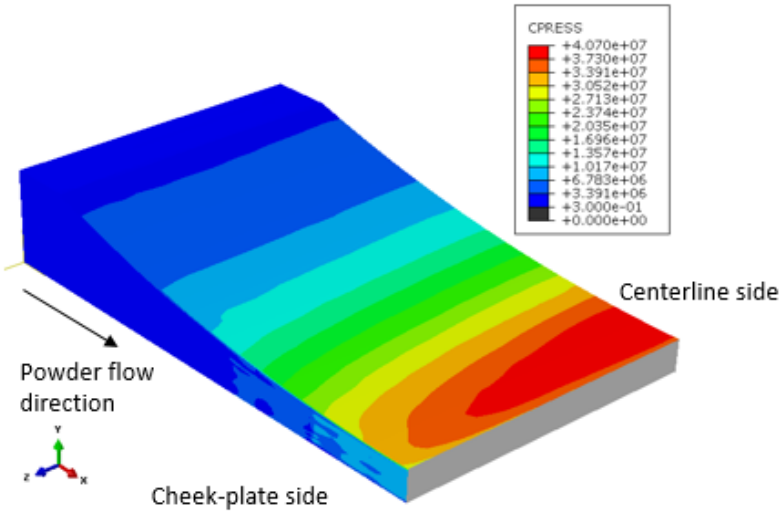

(b)

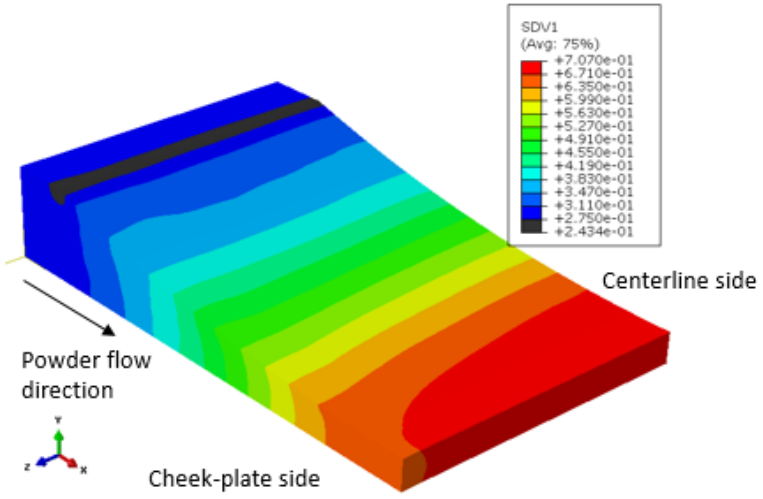

Figure 4.2. (a) Roll normal stress (Pa) and (b) Relative density distributions for the example simulation. The inlet stress, minimum gap width, roll diameter, roll width, powder-roll friction coefficient and powder-cheekplate friction coefficient for this special case are, respectively, 200 kPa, 2 mm, 100 mm, 20mm, 0.35 and 0.35. The remainder of the material properties are given in Tables 3.4 and 3.5.

Figure 4.3 shows the relative density at the minimum gap along the ribbon spanwise direction for four different powder-sideplate frictional cases. The x-axis is the ribbon spanwise location with zero being closest to cheekplate and -0.01 m being the middle of the ribbon. While the boundary is frictionless, the relative density is uniform across the ribbon spanwise direction. On the other hand, it is evident that increasing the powder-sideplate friction results in a smaller density ribbon and greater variation in the ribbon spanwise direction with the highest values in the middle and the lowest in the edges. The results indicates that the powder is not uniformly delivered to the downstream region and the powder-cheekplate friction has a negative influence on the ribbon uniformity. This occurs as the shear stress caused by the side plate friction prevents the powder close to the side plate from flowing downstream and causes an uneven compaction across the ribbon width, with lower densification at the edges.

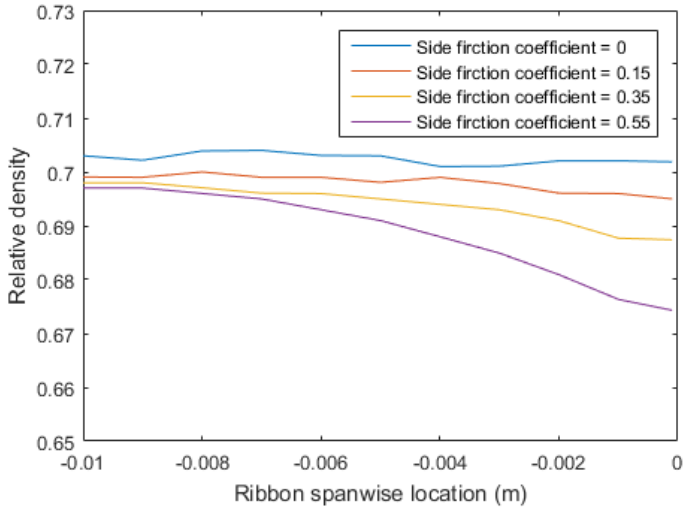

Figure 4.3. Relative density along the ribbon spanwise direction based on distance from the cheekplate (with zero closest to the cheekplate) for different powder-cheekplate friction coefficients. The inlet stress, minimum gap width, roll diameter, roll width, and powder-roll friction coefficient for those cases are, respectively, 200 kPa, 2 mm, 100 mm, 20 mm, and 0.35. The remainder of the material properties are given in Tables 3.4 and 3.5.

Often in reality, the side plates don't extend downstream of the minimum gap width. Hence, a roll compaction system without side plates downstream is also of interest in the current study. The model geometry and boundary conditions in the new model remain the same as those described in Figure 4.1, with the release region extending downstream of the side plates.

An example FEM simulation is shown in Figure 4.4, with the relative density distribution for different streamwise locations plotted in Figure 4.5. As shown in Figure 4.5, The FEM simulation shows a small relative density change, about 3%, between the minimum gap (Position 1, x = 0.016 m) and post-roll (Position 2, x = 0.020 m) compaction relative densities, which represents the spring-back mechanism in the release region. An important point is that Avicel-PH102, the material used here, deforms primarily in a plastic manner and exhibits little elastic rebound according to LaMarche et al. [25], which agrees with the FEM-computed results. The same elastic rebound can be noticed near the edges in the spanwise direction when powders move outside the side plate (downstream of Positions 2 and 3). As shown in Figure 4.6, when powder-cheekplate friction coefficient is sufficiently large (> 0.5), the ribbon will split near the edges once outside the side plate, since the relative density is less than the initial value in the FEM simulations. This might be the reason why side plates are typically manufactured using materials with small friction coefficients.21

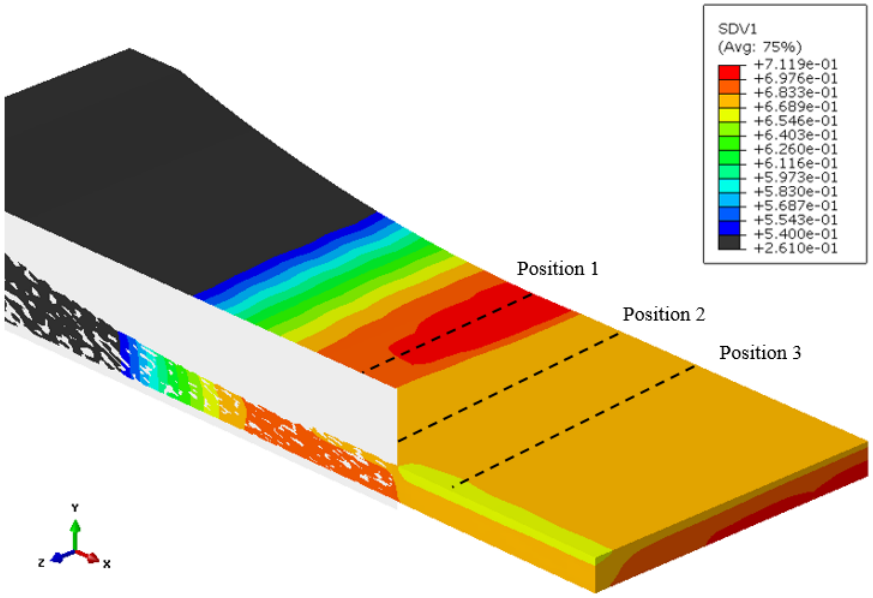

Figure 4.4. Relative density distributions for the example simulation with the release region extending downstream of the side plates. The inlet stress, minimum gap width, roll diameter, roll width, powder-roll friction coefficient, and powder-cheekplate friction coefficient for this special case are, respectively, 200 kPa, 2 mm, 100 mm, 20mm, 0.35, and 0.35. The remainder of the material properties are given in Tables 3.4 and 3.5.

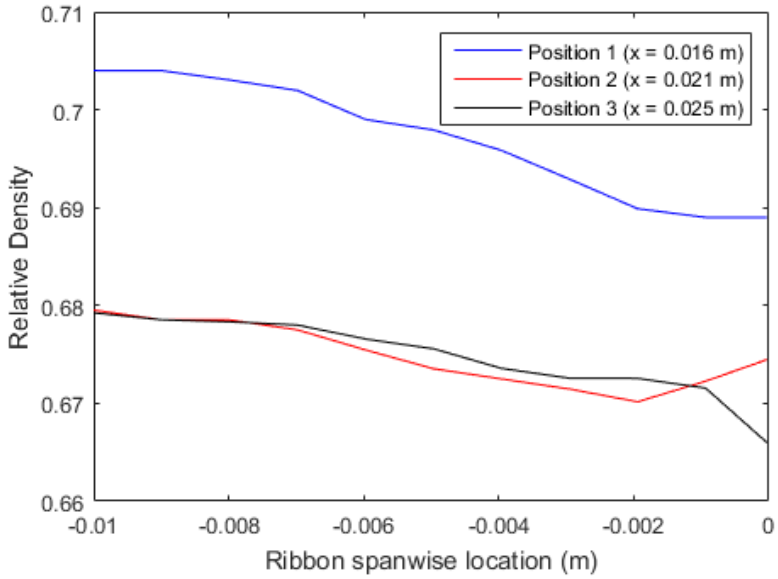

Figure 4.5. Relative density along the ribbon spanwise direction based on distance from the cheekplate (with zero closest to the cheekplate) for different positions shown in Figure 4.4.

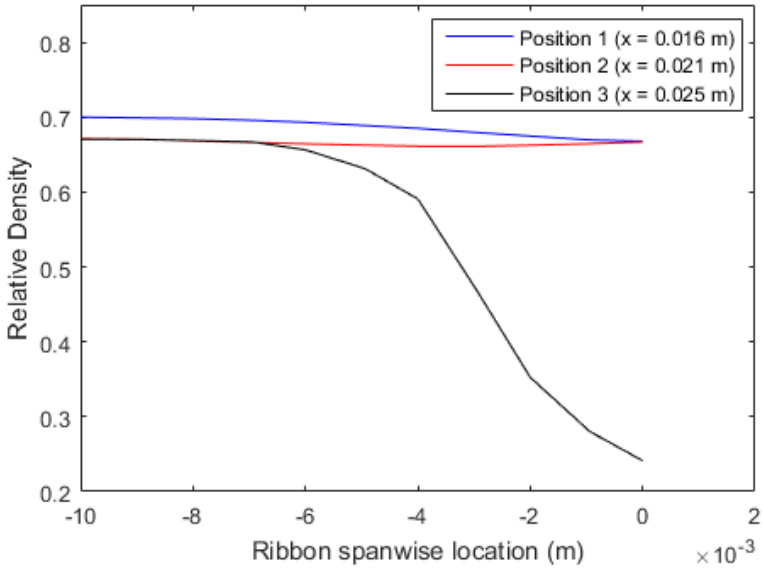

Figure 4.6. Relative density along the ribbon spanwise direction based on distance from the cheekplate (with zero closest to the cheekplate) for different positions with powder-cheekplate friction coefficient being 0.35.

4.4 Conclusions

In this chapter, a three-dimensional Finite Element Method (FEM) model is developed to provide insights into the roll compaction process. The simulation results clearly show that a larger powder-cheekplate friction coefficient results in a smaller and more non-uniform density distribution, with the largest values in the middle and the smallest at the edges. Also, downstream of the rolls elastic rebound of the ribbon in both directions can be noticed in the FEM simulation result. The results demonstrate the capability of FEM modeling to provide insight and help achieve a better understanding of the roll compaction process.

CHAPTER 5. THE MODIFIED JOHANSON MODEL

5.1 Introduction

The two-dimensional FEM simulations in Chapter 3 indicate that the one-dimensional flow assumption in the Johanson model is improper and can lead to an over-prediction of the ribbon relative density at the minimum gap. Hence, the Johanson model is modified in this Chapter to include the influence of the non-uniform velocity profile and provide a better prediction of the ribbon relative density. In order to validate the modified Johanson model, predictions from this modified model are compared to FEM simulation results and published experimental data in this chapter

5.2 Model Derivations

5.2.1 Slip Region

The Johanson model [2] divides flow through the roll compactor into two regions: a slip region located near the inlet where powder slips against the roll surfaces, and a no-slip region located downstream of the slip region where powder is assumed to have a streamwise speed equal to the roll periphery speed. Johanson's approach to modeling the stresses in the slip region and the nip angle remain unchanged in the current work and is derived here for convenience.

In order to determine the stress distribution in this region, the stress at the inlet boundary to the slip region is required as an input parameter. Typically, a feed screw is

located upstream of the inlet and is used to feed powder to the roll. However, Johanson assumed that a uniform minor principle stress σ_h, i.e., $\sigma_h = \sigma_2$ with no shear stress on the surface, is applied at a pre-defined inlet plane. The position angle, θ_h, and the distance from the roll centers, h, for the inlet plane may be found using a Mohr's circle (Figure 5.1),

$$\theta_h = \left(\frac{1}{2}\pi - 2\nu\right), \tag{5.1}$$

$$h = \frac{1}{2} D \sin\theta_h, \tag{5.2}$$

where υ is the actual angle as shown in Figure 5.1 and defined as,

$$2\nu = \pi - \arcsin\frac{\sin\phi'}{\sin\delta} - \phi'. \tag{5.3}$$

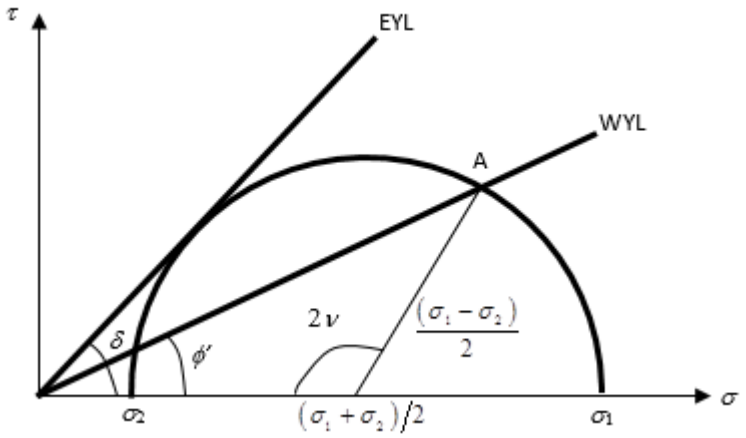

Figure 5.1. Mohr's circle

The pressure at the inlet may also be found from the Mohr's circle geometry,

$$P_h = \frac{\sigma_h}{1 - \sin\delta}. \tag{5.4}$$

Using the method of characteristics to get a first-order approximation, the pressure distribution in the slip region along the centerline of the symmetry is then found by Johanson to be,

$$\frac{d\left(P_\theta/P_h\right)}{d\left(x/D\right)}=\frac{-8\left(P_\theta/P_h\right)\left(\frac{\pi}{2}-\theta-\nu\right)\tan\delta}{\left(1+\frac{S}{D}-\cos\theta\right)\left[\cot\left(A-\mu\right)-\cot\left(A+\mu\right)\right]}, \tag{5.5}$$

where $A=\frac{1}{2}\left(\theta+\nu+\frac{\pi}{2}\right)$ and $\mu=\frac{\pi}{4}-\frac{\delta}{2}$.

This pressure gradient may be integrated numerically starting at the inlet boundary to determine the pressure throughout the slip region.

5.2.2 No-Slip Region

In the no-slip region, Johanson assumed that the powder velocity is one-dimensional. Hence, from conservation of mass, the mass contained within a small volume at the nip angle α, i.e., the angle dividing the slip and no-slip, is the same mass at any other location, θ, in the no-slip region (Figure 5.2),

$$\eta_\theta V_\theta=\eta_\alpha V_\alpha, \tag{5.6}$$

where η is the powder relative density. The parameter V is a small volume element given by,

$$V_\theta=\left[S+D\left(1-\cos\theta\right)\right]\cos\theta\Delta L W, \tag{5.7}$$

where S is the minimum gap width between the rolls, D is the roll diameter, ΔL is a small displacement around the roll surface, and W is the depth of the roll into the page (roll width).

In order to relate the powder relative density to the applied pressure, a constitutive relation is required. Johanson assumed the following relation based on empirical observations,

$$\frac{P_\theta}{P_\alpha} = \left(\frac{\eta_\theta}{\eta_\alpha} \right)^K , \tag{5.8}$$

where P is the pressure and K is a fitting constant.

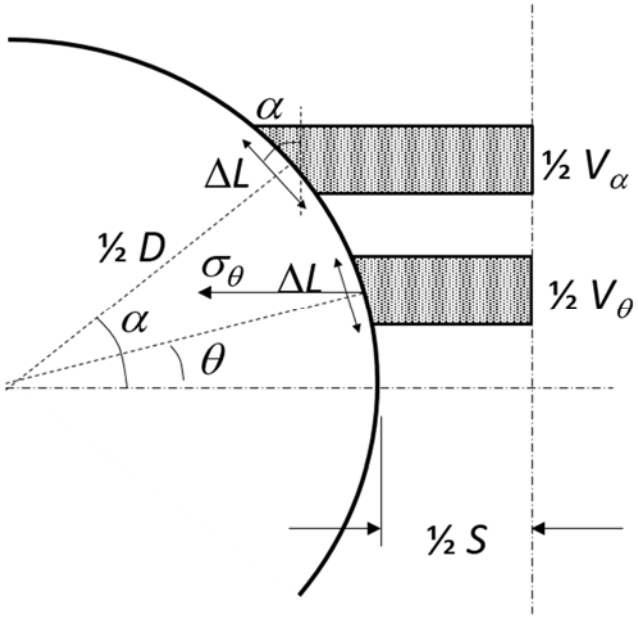

Figure 5.2. A schematic showing powder volume elements in the no-slip region.

Combining Equations (5.6) - (5.8) gives the pressure in the no-slip region,

$$P_\theta = P_\alpha \left[\frac{\left(1 + S/D - \cos\alpha\right)\cos\alpha}{\left(1 + S/D - \cos\theta\right)\cos\theta} \right]^K , \tag{5.9}$$

where the pressure at the nip angle P_α is found by integrating the pressure gradient in the slip region (refer to [2]). Also, by equaling the pressure gradient in both slip region and no-slip region and numerically solving it, the nip angle α can be determined.

Because the pressure is known at every angle, the roll force and torque may be calculated. Typically the pressure in the no-slip region is much larger than the pressure in the slip region so only the pressure contribution in the no-slip region is considered in the calculations. For example, the roll force, *F*, is,

$$F \approx \int_{\theta=0}^{\theta=\alpha} \sigma_\theta W \frac{1}{2} D \cos\theta d\theta , \tag{5.10}$$

where,

$$\sigma_\theta = P_\theta \left(1+\sin\delta\right), \tag{5.11}$$

is the maximum normal stress on the roll's surface projected in the y direction (Figure 5.2) and δ is the powder's effective angle of internal friction. Equations (5.9) - (5.11) may be combined to give the roll force in terms of the maximum pressure P_0 at the minimum gap location ($\theta = 0$),

$$F \approx P_0 \left(1+\sin\delta\right) W \frac{1}{2} D \int_{\theta=0}^{\theta=\alpha} \left[\frac{S/D}{\left(1+S/D-\cos\theta\right)\cos\theta} \right]^K \cos\theta d\theta . \tag{5.12}$$

5.2.3 Mass Correction Factor

A significant assumption in the Johanson model is that the flow is one-dimensional in the no-slip region. However, FEM simulations, such as the one shown in Figure 3.3, indicate that the powder speed is faster at the roll surface than it is at the centerline. This observation has been reported previously [5,7,14,15]. Since the Johanson model assumes that the streamwise speed is equal to the streamwise projected roll speed at each cross-section, the model will over-predict the powder relative density.

Bi et al. [16] included a mass correction factor f_θ in the mass conservation equation (Equation (5.6)) in order to account for the fact that the mass in each of the elements may vary due to multi-dimensional flow,

$$\eta_\theta V_\theta = f_\theta \eta_\alpha V_\alpha . \tag{5.13}$$

Including this mass correction factor in the derivation, the resulting pressure in the no-slip region is,

$$P_\theta = P_\alpha \left[\frac{f_\theta \left(1 + S/D - \cos\alpha\right)\cos\alpha}{\left(1 + S/D - \cos\theta\right)\cos\theta} \right]^K . \tag{5.14}$$

In addition, incorporating the mass correction factor into Equation (5.12) gives,

$$F \approx P_0 \left(1 + \sin\delta\right) W \frac{1}{2} D \int_{\theta=0}^{\theta=\alpha} \left(\frac{f_\theta}{f_0} \right)^K \left[\frac{S/D}{\left(1 + S/D - \cos\theta\right)\cos\theta} \right]^K \cos\theta d\theta . \tag{5.15}$$

Note that Eq. (5.15) is different than the one derived by Bi et al. [16]. The Bi et al. derivation (their Equation (15)) had f_0^K as the pre-factor within the integral, which appears to be a derivation mistake. Bi et al. determined f_0 by back-fitting roll force measurements from one experiment, then found that this same value worked well for other operating conditions using the same formulation. They noted that f_0 varied between 0.86 and 0.89 for their experiments. Also, it was mentioned in their work that they could not figure out how to predict f_0, which is discussed in the current study.

Equation (5.15) indicates that the angular dependence of the mass correction factor must be known. The FEM simulations were used with Equation (5.13) to determine this functional form. The nip angle for this calculation was found directly from the unmodified Johanson model since prior work [5,12] has shown that the Johanson model is reasonably accurate for this calculation. The mass correction factor normalized

by the mass correction factor at the minimum gap width ($\theta = 0$) is plotted as a function of angular position normalized by the nip angle in Figure 5.2 for a range of boundary conditions (gap width-to-roll diameter, inlet stress, and powder-roll friction coefficient), which are identified in Table 5.1. Interestingly, this curve varies little over a wide range of parameters. A curve of the form,

$$\frac{f_\theta}{f_0} = 1 + \frac{1 - f_0}{f_0}\left(\frac{\theta}{\alpha}\right)^n, \tag{5.16}$$

is proposed to fit the FEM data. Note that this fit has three parameters: the nip angle α, the mass correction factor at the minimum gap f_0, and the exponent n. The nip angle is determined from the unmodified Johanson model, as described previously. As shown in Figure 5.3 and Table 5.1, the exponent n is independent of boundary conditions. Additional FEM simulations show that the exponent n varies with the material properties. Bi et al.'s experiments provide similar observations [16]. For example, the current study uses Avicel PH-102 (FMC-BioPolymer, PA, USA), which gives a best fit to Equation (5.16) when n = 1.25. Additional FEM simulations using the DPC properties for lactose (Foremost Fast Flo 316) give n = 1.75. Determination of the mass correction factor at the minimum gap width is described in the following paragraphs.

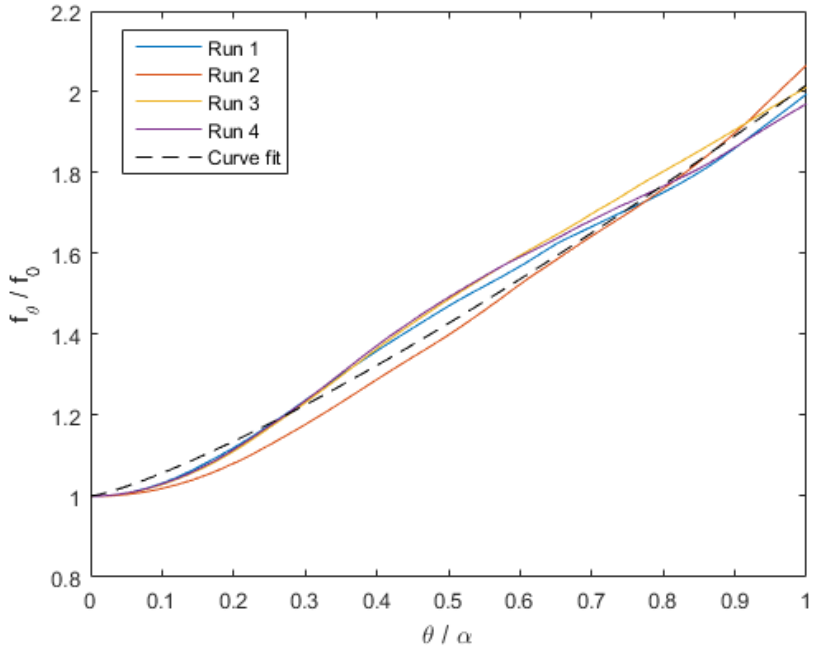

Figure 5.3. The mass correction factor normalized by the mass correction factor at $\theta = 0$ plotted as a function of angular position normalized by the nip angle as measured from FEM simulations (Table 5.1). The curve fit proposed in Equation (5.16) is shown as a dashed line.

Table 5.1. Detail boundary conditions for different runs in Figure 5.3. The material properties are given in Tables 3.2 and 3.3.

Run #	Inlet stress (kPa)	Minimum gap width (mm)	Roll diameter (mm)	Powder-roll friction coefficient
1	200	4	200	0.35
2	100	4	200	0.5
3	200	4	200	0.5
4	100	2	200	0.5

5.2.4 Ribbon Relative Density

The mass correction factor fitting equation is substituted into Equation (5.15) to give,

$$\frac{F}{\frac{1}{2}DWP_0\left(1+\sin\delta\right)} \approx \int_{\theta=0}^{\theta=\alpha}\left[1+\frac{1-f_0}{f_0}\left(\frac{\theta}{\alpha}\right)^n\right]^K\left[\frac{S/D}{\left(1+S/D-\cos\theta\right)\cos\theta}\right]^K \cos\theta d\theta, \quad (5.17)$$

where the pressure at the minimum gap width ($\theta = 0$) is,

$$P_0 = P_\alpha\left[\frac{f_0\left(1+S/D-\cos\alpha\right)\cos\alpha}{S/D}\right]. \quad (5.18)$$

As stated previously, the nip angle α and pressure at the nip angle P_α are calculated using the unmodified Johanson model. In Table 5.2, which lists FEM-computed and unmodified Johanson model values for α and P_α, the unmodified Johanson model is shown to be reasonably accurate at providing the nip angle while the pressure at the nip angle is slightly higher than the simulation result. As discussed below, this difference can lead to a slightly larger prediction of ribbon relative density. Note that in Equation (5.16) the mass correction factor at the minimum gap width, f_0, must be known. Commercial roll compactors typically operate with roll force or roll gap control. In either case, the force acting on the rolls is usually reported. Thus, Equations (5.17) and (5.18) may be used to solve for f_0.

Table 5.2. Comparison of nip angle and pressure at nip angle predictions between FEM model and the Johanson model. The inlet stress, minimum gap width, roll diameter, and powder-roll friction coefficient are, respectively, 200 kPa, 4 mm, 200 mm and 0.50. The remainder of the material properties are given in Tables 3.2 and 3.3.

	Nip angle α (degree)	Pressure at the nip angle P_α (MPa)
FEM model	18.54	4.10
Johanson model	18.33	5.91

Although in the current study the exponent n for a certain material is derived directly from FEM simulation results, it is not necessary to run FEM simulations to determine this value. If the ribbon density is measured in an experiment in which the roll force and roll gap are also known, then the fit parameters (n, f_0) can be determined. For example, from the ribbon density, the maximum pressure can be calculated from the pressure-relative density relation (Equation (5.8)), assuming the compressibility exponent is known from separate characterization experiments. The mass correction factor at the minimum gap width can then be found from Equation (5.18) since the pressure at the nip angle (as well as the nip angle itself) may be calculated from the original Johanson analysis. Note that like the compressibility exponent, the effective internal friction angle is assumed known from characterization experiments. Lastly, the exponent n in the mass correction expression can be found using Equation (5.17) since the roll force is known.

The compressibility constant K used in the Johanson model is normally found from punch and die experiments. In the current work, this K is derived directly from the cap hardening parameters of the DPC model (Table 3.3) where the relative density can be derived from the total volumetric plastic strain through Equation (3.1). Figure 5.4 plots the pressure as a function of the relative density for Avicel PH-102 on a log-log axis. The data is fit well using,

$$\frac{P}{P_{\text{initial}}} = \left(\frac{\eta}{\eta_{initial}} \right)^{K}, \tag{5.19}$$

where $\eta_{\text{initial}} = 0.311$ is the inlet relative density (tapped relative density as mentioned previously) used in the FEM simulation and $P_{\text{initial}} = 378.5$ kPa is the corresponding pressure according to the fit data. The compressibility (fitting) constant for this case is K

= 5.08. Compressibility constants between 4.5 and 5.9 were reported by Bi et al. [16] in their experiments using formulations consisting of several materials, including Avicel PH-102. Nesarikar et al. [22] also reported compressibility constants of between 4 and 6 in their formulations, which contained equal amounts of Avicel PH-102 and lactose as well as other components.

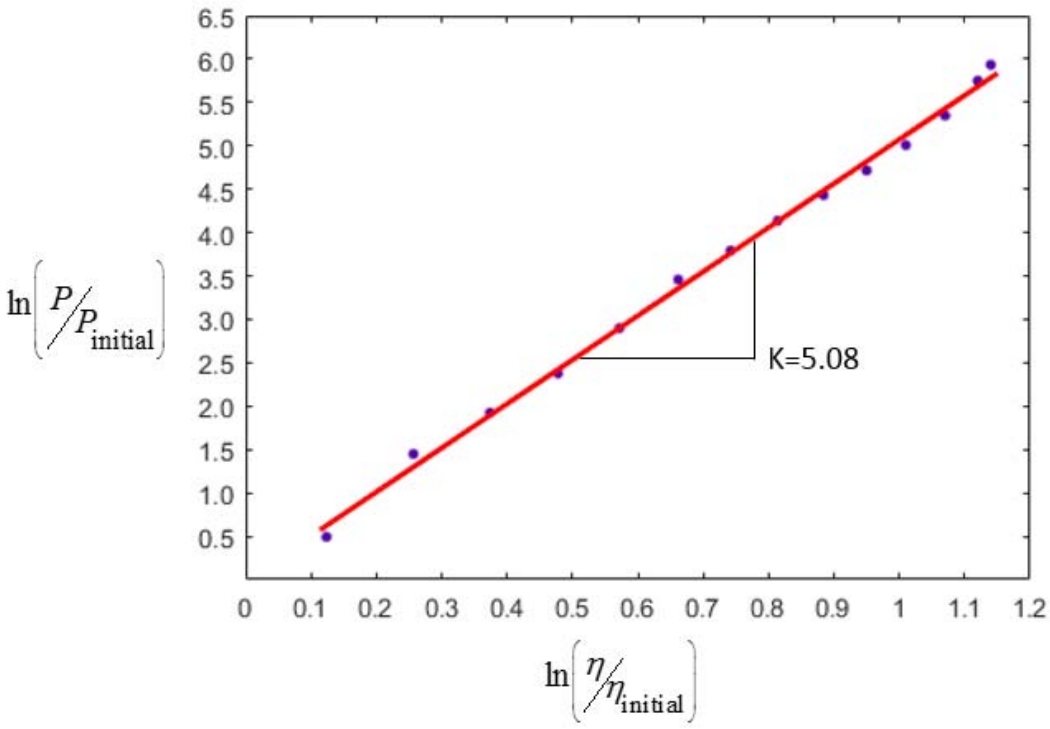

Figure 5.4. Pressure-density relation of Avicel PH-102 from density-independent cap hardening parameters (Table 3.3).

In addition to the pressure-density relation, the effective angle of internal friction δ used in the Johanson model is also determined from the DPC properties. The Mohr-Coulomb model used in Johanson's model assumes a linear relationship between shear and normal stresses at the shear yield surface while the Drucker-Prager Cap model used

in the FEM simulations assumes a linear relationship between the deviatoric stress and pressure. Previous efforts [21,23,24] attempted to develop relationships between the Mohr-Coulomb parameters and the DPC parameters using a variety of approaches, such as matching plane strain response, triaxial test response, or different strength criteria. Most of these relations are not suitable for large friction angles, including the one used by Muliadi et al. [5]. Thus, the current work modifies the relations originally developed by Pistrol et al. [23] since it can handle DPC friction angles up to $\beta = 70°$ (refer to the Appendix). The resulting relationship between the effective angle of internal friction δ used in the Mohr-Coulomb model and the angle of friction β in the DPC model is,

$$\sin\delta = \frac{3}{6+\tan\beta}\left(\frac{d}{P_{\text{initial}}}+\tan\beta\right), \tag{5.20}$$

Through Equations (5.17) and (5.18), the pressure at minimum gap P_0 can be derived once the mass correction factor at the minimum gap, f_0, and the exponent, n, are determined. Then Equation (5.19) can be used to determine the ribbon relative density at the minimum gap, η_0, directly from the P_0.

5.3 Results and Discussion

5.3.1 Input Parameters

To ensure a consistent comparison between the FEM model and Johanson model, the material properties and boundary conditions of Johanson model are derived from FEM simulations directly. The roll geometry, inlet pressure, and powder-roll friction angle are identical to those used in the FEM system. The material properties are determined using the methods described in Chapter 5.2.4.

5.3.2 Comparisons and Discussion

Table 5.3 shows the comparisons between FEM model, the Johanson model and modified Johanson model. The predictions of maximum pressure and average relative density at the minimum gap using the Johanson model are much larger than the FEM-computed results, as mentioned previously. In fact, the relative density predicted by the Johanson model is even unphysical since it is greater than one. On the other hand, predictions of the relative density from the modified Johanson model are compared to predictions from two-dimensional FEM models and the errors are found to be less than 5%. Hence, considering the mass correction factor, the modified Johanson model improves the relative density predictions significantly.

Table 5.3. Comparison between predictions of FEM model, Johanson model and modified Johanson model. The inlet stress, minimum gap width, roll diameter, and powder-roll friction coefficient are, respectively, 200 kPa, 4 mm, 200 mm and 0.35. The remainder of the material properties are given in Tables 3.2 and 3.3.

	Mass correction factor f_0	Error	Maximum Pressure P_0 (Pa)	Error	Relative density at the minimum gap η_0	Error
FEM model	0.771	N/A	3.49E+07	N/A	0.762	N/A
Johanson model	N/A	N/A	2.18E+08	524%	1.089	43%
Modified Johanson model	0.751	-2.58%	4.26E+07	22%	0.789	3.57%

Figure 5.5 plots the relative density at the minimum gap width predicted using the two-dimensional FEM model, the original Johanson analysis, and the modified Johanson

analysis described previously. A range of values for the powder-roll friction coefficient and roll geometry are shown. The remainder of the system parameters are given in the figure caption. All of the models predict similar trends, e.g., increasing ribbon relative density as powder-roll friction coefficient increases and dimensionless roll gap width decreases. Larger powder-roll friction coefficients produce larger shear stresses at the boundaries, which in turn increase the material plastic strain and the relative density (refer to Equation (3.1)). Muliadi et al. [5] reported a similar trend. Smaller dimensionless gap widths also increase the amount of material plastic strain and relative density due to decreasing flow area.

Of particular note in Figure 5.5 is that the original Johanson model gives much larger values than the modified model and FEM simulations. Moreover, in most cases the original Johanson predictions are unphysical, with ribbon relative densities greater than one. The modified Johanson model gives reasonable predictions that are approximately 5% larger than the FEM results, with mass correction factors ranging from 0.5 to 0.9. This slight over-prediction in relative density occurs because the pressure at the nip angle P_α in the modified Johanson model is derived directly from the unmodified model and is slightly larger than the FEM value. Clearly, accounting for multi-dimensional flow via a mass correction expression greatly improves the accuracy and usefulness of the Johanson model.

(a)

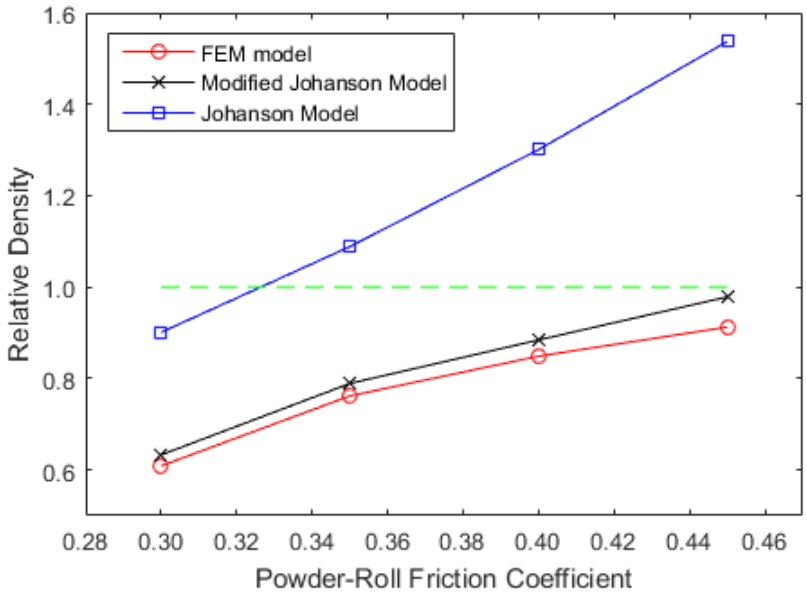

(b)

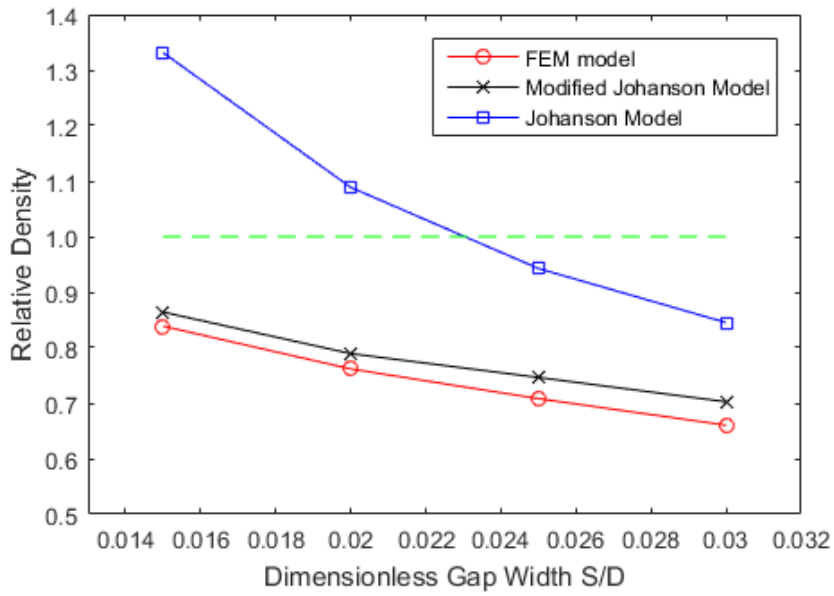

Figure 5.5. Maximum relative densities as functions of (a) powder-roll friction coefficient and (b) dimensionless gap width S/D. The inlet stress, minimum gap width, roll diameter, and powder-roll friction coefficient are, respectively, (a) 200 kPa, 4 mm, 200 mm, N/A and (b) 200 kPa, N/A, 200mm, 0.35. The remainder of the material properties are given in Tables 3.2 and 3.3.

Additional FEM simulations were developed in order to determine how density-dependent DPC properties and three-dimensional flow change the accuracy of the modified Johanson model. First, a three-dimensional, density-independent FEM model with frictionless cheekplates was compared to the two-dimensional results. As summarized in Table 5.4, the two-dimensional model gives accurate predictions as compared to the three-dimensional model, with relative differences of less than 1%. The three-dimensional FEM simulations, however, require far more computational resources, with wall clock times approximately 10 times larger than those for the two-dimensional simulations.

Table 5.4. Comparison between three-dimensional FEM model and two-dimensional FEM model. The inlet stress, minimum gap width, roll diameter, and powder-roll friction coefficient are, respectively, 200 kPa, 4 mm, 200 mm and 0.35. The remainder of the material properties are given in Tables 3.2 and 3.3.

	Maximum pressure P_0 (Pa)	Error	Relative density at the minimum gap η_0	Error
3D FEM model	3.20E+07	N/A	0.751	N/A
2D FEM model	3.18E+07	-0.63%	0.747	-0.53%

Next, several three-dimensional, density-dependent FEM simulations, as described in Chapter 4, were performed in which the powder-cheekplate friction coefficient was varied with values between 0 and 0.55. The compressibility constant and effective angle of internal friction used in the modified and original Johanson models were found using the procedures described in Chapter 5.2.4, but using the density-dependent DPC properties (Tables 3.4 and 3.5). Note here the effective angle of internal

friction was derived from the average friction angle in the DPC model over the range of all relative densities using Equation (5.20). Figure 5.6 shows that the proposed mass correction factor relation (Equation (5.16)) is still a good fitting equation; however, for the same material, the exponent n increases with increasing powder-cheekplate friction coefficient. For a sufficiently small friction coefficient (< 0.3), the exponent *n* derived from two-dimensional simulations is still a good mass correction factor value, giving errors of less than 10% from the value fit from the three-dimensional simulations.

(a)

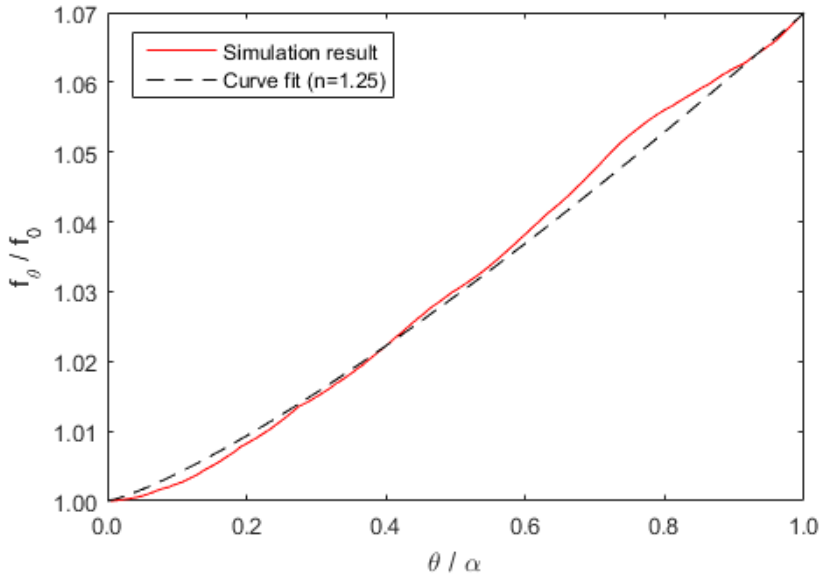

Figure 5.6. The mass correction factor normalized by the mass correction factor at $\theta = 0$ plotted as a function of angular position normalized by the nip angle as measured from FEM simulations for powder-cheekplate friction coefficient of (a) 0.15 and (b) 0.35. The curve fits proposed in Equation (12) for different exponent n are shown as dashed lines. The inlet stress, minimum gap width, roll diameter, roll width and powder-roll friction coefficient are 200 kPa, 2 mm, 100 mm, 20 mm, and 0.35. The remainder of the material properties are given in Tables 3.4 and 3.5.

(b)

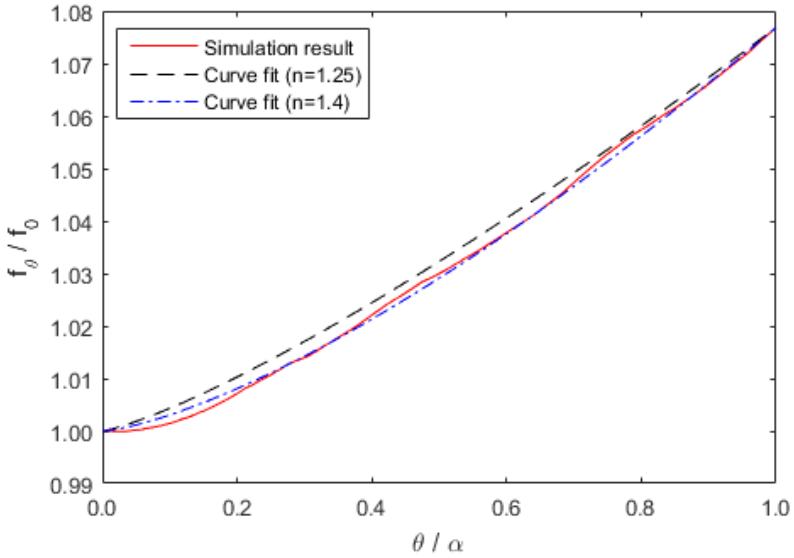

Figure 5.6. Continued.

Lastly, the published experimental results of Cunningham [7] were compared to predictions from two-dimensional, density-dependent FEM simulations and the modified Johanson model. The material used in both the experiments and simulations was Avicel PH-102 (DPC data in Tables 3.4 and 3.5). Note that in the FEM simulation, the powder-roll friction coefficient, which is a prescribed value in the modified Johanson model, is fitted to give the same roll force value as the experiment results since this coefficient was not reported in Cunningham's work. An important point is that the Cunningham ribbon relative density measurement is for the ribbon downstream of the minimum gap width, which means that the relative density includes the effects of elastic springback. Avicel-PH102, the material used here, deforms primarily in a plastic manner and exhibits little elastic rebound according to LaMarche et al. [25]; however, it is not zero. As shown in

Table 5.5, The FEM simulations show a small relative density change, less than 3%, between the minimum gap and post-roll compaction relative densities. The post-roll compaction relative density predicted by the FEM model is within 1% of the experimental measurement, indicating an excellent prediction. The modified Johanson model prediction, which provides only a minimum gap relative density prediction, is approximately 2% larger than the corresponding FEM model prediction and less than 5% larger than the post-roll compaction experimental result. Thus, we conclude that the modified Johanson model gives accurate results. If materials that have a larger elastic response, such as lactose, are roll compacted, then the modified Johanson model prediction of the minimum gap width relative density could be potentially much larger than the actual post-roll compaction value.

Table 5.5. Comparison of relative density predictions between experiment, FEM model (with density-dependent DPC properties) and modified Johanson model.

	Roll Gap (mm)	Roll Force (N/mm)	Relative density at the minimum gap η_0	Ribbon Relative Density η_{ribbon}
Experiment	1.89	242.9	N/A	0.636
FEM model	2	227.1	0.6522	0.6335
Modified Johanson model	2	227.1	0.6655	N/A

5.4 Conclusions

In this chapter, Johanson's analysis is modified to include a mass correction factor to account for his improper one-dimensional flow assumption, similar to what was proposed by Bi et al. [16]. Unlike Bi et al.'s work, however, an empirical curve fit for the mass correction factor is included in the current analysis. Two fitting parameters, found

from an on-line measurement of the roll force, can be used to determine the mass correction factor at the minimum gap width.

Relative density predictions of the modified Johanson model are compared to simulation results from two-dimensional FEM models and the errors are found to be around 5% of the FEM predictions while the unmodified Johanson model overpredicts the results by around 50%. Comparisons to published experimental data also show good agreement. Moreover, when considering the powder-cheekplate friction in 3D FEM models, the exponent *n* derived from two-dimensional simulations is still a good mass correction factor value for a reasonably small friction coefficient (< 0.3).

Hence, the mass-corrected modified Johanson model can provide much more accurate predictions of the relative density at the minimum gap than the unmodified Johanson model. This modified Johanson model can be used in control schemes to provide much better estimates of ribbon relative density in roll compaction operations.

CHAPTER 6. CONCLUSIONS AND FUTURE WORK

6.1 Conclusions

The focus of this work is to modify Johanson's analytical model to improve predictions of the maximum bulk relative density. Studies [1] have reported that the resulting product properties, such as disintegration and compact strength, are determined mainly by the ribbon bulk density. Prior work [5] has shown that Johanson's roll compaction model over-predicts, and in some cases, provides unphysical values for a ribbon's relative density. This inaccuracy has been shown to be due to the one-dimensional flow assumption in the model. Bi et al. [16] proposed the use of a mass correction factor to account for multi-dimensional flow effects; however, the expression reported in their publication has derivation errors. In the present work, a mass correction approach is also used, but unlike Bi et al.'s work, the dependence of the mass correction factor on position within the roll compactor is accounted for.

Two-dimensional and three-dimensional finite element method simulations are used in the current study to provide insights into the form of the mass correction factor relation and a means of computational validation. The resulting prediction of minimum gap ribbon relative density is shown to be only a few percent larger than FEM-predicted relative densities. Like the original Johanson's model, predictions from this modified model can be quickly calculated and, thus, is well suited for control system.

The empirical mass correction factor relation proposed here (Equation (5.16)) has two fitting parameters: a power constant n and the mass correction factor at the minimum gap width f_0. Using measurements of the roll force and minimum gap width, which are often reported in commercial roll compaction equipment, these fitting parameters can be determined. The value for n is shown to be independent of powder-roll friction coefficient and dimensionless gap width, but does depend on the compaction properties of the material and the powder-cheekplate friction coefficient. Once the value of n is determined, the parameter f_0 is then just a function of the roll force. Also, although in the current study the exponent n for a certain material is derived directly from FEM simulation results, it is not necessary to run FEM simulations to determine this value. If the ribbon density is measured in an experiment in which the roll force and roll gap are also known, then the fit parameters (n, f_0) can be determined.

The current work also shows that the material properties and roll geometries can affect the two-dimensional velocity gradients, thus affect the deviations from Johanson's original model. According to the FEM simulations, increasing powder-wall and powder-cheekplate friction coefficient can result in a larger velocity gradient due to the increase in shear stress-included consolidation. Also, increasing the effective angle of internal friction and decreasing the dimensionless gap width, i.e., S/D, can result in a larger velocity gradient, thus more deviations from Johanson's original model.

It need to be mentioned this modified Johanson's model still has its own weaknesses, for example, the predictions of nip angle and pressure at nip angle are directly from Johanson's original model and can introduce some errors. Nevertheless, it has to be recognized the modified Johanson's model is only a one-dimensional model and

therefore has its own limits. Still, it can give us a much more accurate prediction of ribbon relative density than the original model's prediction.

6.2 Recommendations for Future Work

As mentioned before, this modified Johanson's model still has some weaknesses; hence, several improvements to it should be considered in future studies.

First, following Johanson's original model, the modified model assumes a constant normal stress as the input boundary condition. In reality, a feed screw is located upstream of the slip region and used to feed powder to the rolls. Therefore, a more realistic input boundary conditions may be introduced rather than normal stresses. Recently, Timothy's work [9] has shown that the Solid Plug model, i.e., the model used to predict the outlet stress of screw feeders, were orders of magnitude below the experimental measurements and able to be fitted to the experimental results using either the stress ratios or friction coefficients as fitting parameters. Hence, a modified Solid Plug model may be developed and used to predict the stress at the inlet of the nip region in a roll compactor.

Second, both original and modified Johanson's model can only take into account the maximum ribbon relative density at the minimum gap. Additional theories may be needed to modify this model to incorporate springback of the ribbon downstream of the minimum gap. Obviously, for different materials this effect could be different, and Johanson's model (or the modified one) will have additional inaccuracies for materials which performs large spring-back after compaction, such as lactose.

Third, as mentioned before, the predictions of nip angle and pressure at nip angle are derived directly from Johanson's model and can introduce some errors. Future

theories may be developed to better determine the nip angle and pressure at the nip angle to add more accuracy to the current modified model.

Fourth, in the current modified model the exponent n for a certain material is derived directly from FEM simulations and the mass correction factor at minimum gap f_0 is derived based on this exponent. Or if the ribbon density is measured in an experiment in which the roll force and roll gap are also known, then the fit parameters (n, f_0) can also be determined. Still, since the online measurement of the ribbon density is much complex, new methods might be introduced to determine parameters n and f_0 a priori from independent models or experiments.

Also, since the current work only compares the modified Johanson's model with published experiment data, more detail experiments can be developed to validate the current modified model.

Then, considering the spanwise variation of the ribbon relative density due to the powder-cheekplate friction, more works can be done to investigate the possibility of fitting spanwise relative density profile from the average relative density predicted by the modified Johanson model. This can help extend the relative density prediction to multi-dimensions.

Finally, works can be done to investigate the yield criteria in FEM simulations. By monitoring the maximum principal stress or mises equivalent stress in the release region, it is possible to detect the failure of the resultant ribbon.

LIST OF REFERENCES

LIST OF REFERENCES

[1] S.G. von Eggelkraut-Gottanka, S.A. Abed, W. Muller, P.C. Schmidt, Roller compaction and tableting of St. John's wort plant dry extract using a gap width and force controlled roller compactor. II. Study of roller compaction variables on granule and tablet properties by a 3×3 factorial design, Pharmaceutical Development and Technology 7 (2002) 447–455.

[2] J.R. Johanson, A rolling theory for granular solids, ASME Journal of Applied Mechanics E32 (1965) 842–848.

[3] V.P. Katashinskii, Analytical determination of specific pressure during the rolling of metal powders, Soviet Powder Metallurgy and Metal Ceramics 10 (1986) 765–772.

[4] G.Y. Gun, S.A. Stebunov, V.P. Katashinskii, Computer modeling and investigation of the metal powder rolling processes, Powder Metallurgy and Metal Ceramics 25 (1986) 8–11.

[5] A.R. Muliadi, J.D. Litster, C.R. Wassgren, Modeling the powder roll compaction process: comparison of 2-D finite element method and the rolling theory for granular solids (Johanson's model), Powder Technology 221 (2012) 90–100.

[6] A.R. Muliadi, J.D. Litster, C.R. Wassgren, Validation of 3-D finite element analysis for predicting the density distribution of roll compacted pharmaceutical powder, Powder Technology 237 (2013) 386–399.

[7] J.C. Cunningham, Experimental studies and modeling of the roller compaction of pharmaceutical powders: PhD Thesis, Drexel University; 2005.

[8] A. Mazor, L.P. Gabdarillas, A.D. Ryck, A. Michrafy, Effect of roll compactor sealing system designs: A finite element analysis, Powder Technology 289 (2016) 21–30.

[9] T.J. Patterson, Prediction of the stress at the inlet of the nip region in a roll compactor: M.S. Thesis, Purdue University; 2014.

[10] A.W. Jenike, R.T. Shield, On the plastic flow of Coulomb solids beyond original failure, JAM 27 (1959) 599-602.

[11] Z. H. Gu, P. C. Arnold, A. G. McLean, Consolidation-related bulk density and permeability models for bulk solids, Powder Technology 72 (1992) 39-44.

[12] G. Bindhumadhavan, J.P.K. Seville, M.J. Adams, R.W. Greenwood, S. Fitzpatrick, Roll compaction of a pharmaceutical excipient: experimental validation of rolling theory for granular solids, Chemical Engineering Science 60 (2005) 3891–3897.

[13] Y.A. Yusof, A.C. Smith, B.J. Briscoe, Roll compaction of maize powder, Chemical Engineering Science 60 (2005) 3919–3931.

[14] A. Zavaliangos, R.T. Dec, R.K. Komarek, Analysis of powder processing in the roller press using finite element modeling, in: XXII International Mineral Processing Congress, Cape Town, South Africa, 2003.

[15] E. Orowan, The Calculation of Roll Pressure in Hot and Cold Flat Rolling, Research on the Rolling of Strip, 1960, pp. 10.

[16] M. Bi, F. Alvarez-Nunez, F. Alvarez, Evaluating and modifying Johanson's rolling model to improve its predictability, J Pharm Sci. 103 (2014) 2062-2071.

[17] A. Michrafy, H. Diarra, J.A. Dodds, M. Michrafy, Experimental and numerical analyses of homogeneity over strip width in roll compaction, Powder Technology 206 (2011) 154–160.

[18] T. Sinha, J.S. Curtis, B.C. Hancock, C.Wassgren, A study on the sensitivity of Drucker–Prager cap model parameters during the decompression phase of powder compaction simulations, Powder Technology 198 (2010) 315–324.

[19] S. Swaminathan, J. Hilden, B. Ramey, C. Wassgren, Modeling the formation of debossed features on a pharmaceutical tablet, Journal of Pharmaceutical Innovation (2016) Unpublished.

[20] A.L. Gurson, Continuum theory of ductile rupture by void nucleation and growth: Part 1—yield criteria and flow rules for porous ductile media, ASME Journal of Engineering Materials and Technology 99 (1977) 2–15.

[21] Abaqus Analysis User's Manual, Hibbitt, Karlsson and Sorensen, Inc., Rhode Island, 2001.

[22] V. Nesarikar, N. Vatsaraj, C. Patel, W. Early, P. Pandey, O. Sprockel, Z. Gao, R. Jerzewski, R. Miller, M. Levin, Instrumented roll technology for the design space development of roller compaction process, Int. J. Pharm. 426 (2012) 116–131.

[23] J. Pistrol, F. J. Falkner, D. Adam, C. Adam, Comparison of constitutive soil models for the simulation of dynamic roller compaction, European Congress on Computational Methods in Applied Sciences and Engineering, J. Eberhardsteiner et al. (eds.), Vienna, Austria (2012).

[24] H. Jiang, Y. Xie, A note on the Mohr-Coulomb and Drucker-Prager strength criteria, Mechanics Research Communications 38 (2011) 309–314.

[25] K. LaMarche, D. Buckley, R. Hartley, F. Qian, S Badawy, Assessing materials' tablet compaction properties using the Drucker–Prager Cap model, Powder Technology 267 (2014) 208–220.

APPENDIX

APPENDIX

For convenience, details of Pistrol et al.'s work [23] relating Mohr-Coulomb and Drucker-Prager Cap parameters are presented here. Two specific states of stress were chosen to match one edge of the Mohr-Coulomb yield pyramid with the Drucker-Prager shear yield cone. The stress at the apex of both models is,

$$\sigma_a = \frac{c}{\tan\phi}, \tag{A.1}$$

where c is the cohesion and ϕ is the angle of internal friction in the Mohr-Coulomb model.

For the case that the Drucker-Prager cone is tangential to the Mohr-Coulomb pyramid at its compression meridian, the yield stress in uniaxial compression can be written as,

$$\sigma_c = \frac{2c}{\sec\phi - \tan\phi}. \tag{A.2}$$

The angle of friction β and the cohesion d of the Drucker-Prager model then can be expressed as,

$$\tan\beta = \frac{3\sigma_c}{3\sigma_a + \sigma_c} = \frac{6\sin\phi}{3 - \sin\phi}, \tag{A.3}$$

$$d = \frac{3\sigma_c}{3\sigma_a + \sigma_c}\sigma_a = \frac{\tan\beta}{\tan\phi}c. \tag{A.4}$$

Those equations are derived by Pistrol et al. since the Drucker-Prager parameters were adjusted to the Mohr-Coulomb parameters in their case. However, in the current work, the Mohr-Coulomb parameters expressed in terms of the (FEM) DPC parameters are desired,

$$\sin\phi = \frac{3\tan\beta}{6+\tan\beta}, \tag{A.5}$$

$$c = \frac{\tan\phi}{\tan\beta} d\,. \tag{A.6}$$

Note that it is the effective angle of internal friction δ in the Mohr-Coulomb model is used in Johanson's model, not the internal friction angle ϕ. The effective internal friction angle δ may be found from the inlet pressure P_{initial} since the corresponding effective yield locus is the upper limit of all stress conditions, as shown in Figure A.1.

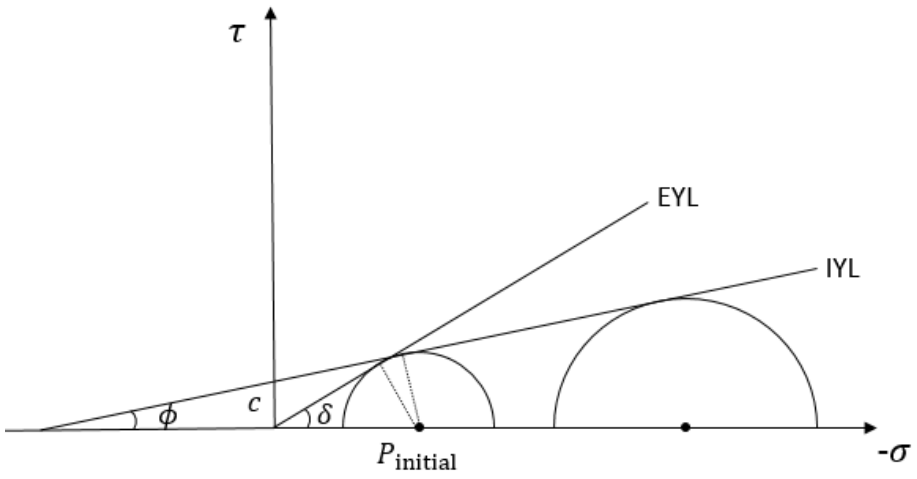

Figure A.1. The effective yield locus and internal yield locus in the σ–τ plane.

According to the geometry in Figure A.1, the effective angle of internal friction δ is,

$$\sin\delta = \left(\frac{c}{P_{\text{initial}} \tan\phi} + 1 \right) \sin\phi \,. \tag{A.7}$$

Substituting Equations (A.5) and (A.6) into Equation (A.7), the final relation between δ and β becomes,

$$\sin\delta = \frac{3}{6 + \tan\beta} \left(\frac{d}{P_{\text{initial}}} + \tan\beta \right). \tag{A.8}$$